Effect of EAM on Quality Factor and Noise in MEMS Vibratory Gyroscopes

Danmeng Wang and Andrei M. Shkel
MicroSystems Laboratory, Department of Mechanical and Aerospace Engineering
University of California, Irvine, CA 92697, USA
Email: {*danmenw, ashkel*}@uci.edu

***Abstract*—This paper reports a study on contribution of electromechanical amplitude modulation (EAM) on performance of MEMS Coriolis vibratory gyroscopes (CVGs). We theoretically predicted and experimentally demonstrated the impact of EAM on both quality factor and output noise in MEMS CVGs operating in the open-loop rate mode. We demonstrated the effect on a dynamically amplified dual-mass gyroscope (DAG) improving the gyroscope performance from 0.04 deg/rt-hr in Angular Random Walk (ARW) and 0.52 deg/hr in bias instability to 0.0065 deg/rt-hr in ARW and 0.08 deg/hr in bias instability by changed the EAM setting from 3.5 to 1.2 V in amplitude and from 75 to 225 kHz in frequency. The optimized EAM parameters were derived by the noise prediction model presented in the paper.**

Keywords: MEMS gyroscopes, dynamic amplification, electrical damping, electromechanical amplitude modulation

I. Introduction

Electromechanical amplitude modulation (EAM) is a widely used technique in capacitive detection of MEMS vibratory devices. It is based on the amplitude modulation of the motional signal by an AC carrier voltage. EAM allows for frequency domain separation between the informational signals and feed-through of the parasitic driving signals [1]–[3], hence, reducing the contribution of the feed-through signal from drive to sense electrodes. Flicker noise, or 1/f noise, in MEMS structures is inversely proportional to the signal frequency, therefore increasing the carrier frequency would also mitigate the noise effect [4]. The motion-induced current in this scheme is proportional to the carrier voltage amplitude and frequency [2], which can affect the signal-to-noise ratio (SNR). The predefined AC carrier potential difference applied to the variable sense capacitor between the movable proof-mass and the anchored electrodes generates a set of harmonics which induces a complex force on the sensor. A component of this force causes electrical damping that impacts the effective quality factor (Q-factor) of the device [5], [6].

EAM capacitive detection scheme in MEMS Coriolis vibratory gyroscopes (CVGs) also affects the Q-factor and output noise of the gyroscopes. The effect can either degrade the performance, when the EAM parameters are incorrectly selected, or improve the performance, when the parameters are appropriately chosen.

This material is based on work supported by the Defense Advanced Research Projects Agency and U.S. Navy under contract No. N66001-16-1-4021.

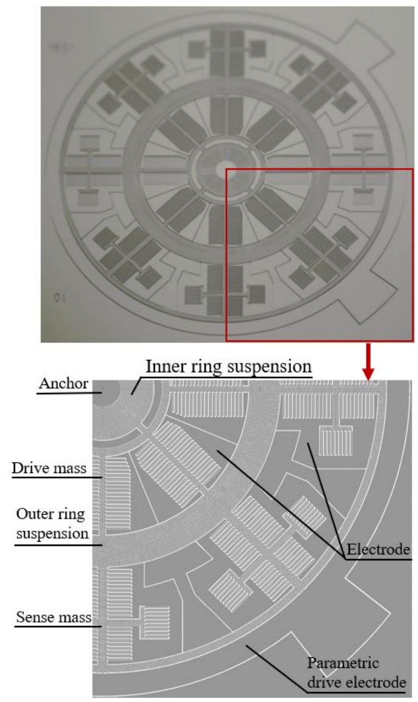

Fig. 1. A image of the dynamically amplified dual-mass gyroscope (DAG) and a close-up image of a quarter of the DAG showing the central anchor, dual-mass, concentric ring suspensions, inner, outer, and parametric electrodes [7], [8].

This paper focuses on studying the effect of EAM using a dynamically amplified dual-mass gyroscope (DAG) as a test vehicle [9], shown in Fig. 1. The impact of the carrier voltage and frequency on electrical damping was theoretically studied and experimentally demonstrated. Additionally, an enhanced noise model for operating CVGs in the open-loop rate mode was presented in this paper. It allows for a prediction and optimization of the DAG by selecting the appropriate control electronics parameters for a given characterization setup.

II. Effect of EAM on Q-Factor tuning

Methods for modification of electrical dissipation as a Q-factor tuning method in micro- and nano-electromechanical resonators were widely reported in recent years [10], [11]. Variations in the amplifier feedback resistance, DC voltage of bias signal, and parasitic capacitance showed great influence on the electrical damping of a doubly clamped micromechan-

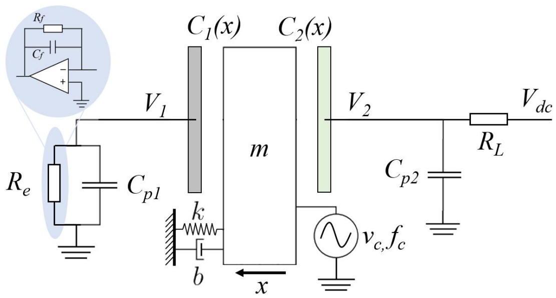

Fig. 2. The equivalent mass-spring system for modeling Q-factor in EAM scheme. $V_c = v_c cos(\omega_c t + \phi)$ is the AC bias applied on the proof-mass. A low-noise transimpedance amplifier (TIA) with feedback resistor, R_f, is used to collect the motional current from the pick-off electrode. Parameters R_e and C_{p1} denote the effective equivalent resistance and capacitance loads attached to the electrode. The actuation voltage, $V_{dc} + V_{ac}(t)$, is applied on the mass via a resistive load, R_L, and a parasitic capacitance, C_{p2}.

ical beam resonator [6]. Application of DC bias voltages to CVG systems has been already widely used in the whole angle gyroscope mode of operation for reduction of the angle drift caused by the Q-factor mismatch [12]. This section is concerned with deriving how the EAM parameters can be modified to tune the effective Q-factor of the open-loop rate gyroscopes.

A. Electrical Damping

Fig. 2 depicts the equivalent system for a mass-spring structure with the EAM capacitive detection setup. An AC carrier signal with amplitude v_c and frequency ω_c is applied to the proof-mass, m. The resonator's displacement is assumed to be $x(t) = xsin(\omega_d t)$. The equivalent resistance load is defined as $\frac{1}{R_e} = \frac{A_{OL}(f)+1}{Z_f} + \frac{1}{Z_{in}}$, where $A_{OL}(f)$, Z_f, and Z_{in} are the open-loop gain, feedback impedance, and input impedance of the TIA, respectively. An ideal drive or sense mode of a CVG can be described by a mass-spring system and presented as

$$m\ddot{x} + b\dot{x} + kx = F_{th} + F_{e1} + F_{e2} \quad (1)$$

The electrical forces in this model, F_{e1} and F_{e2}, are induced by the equivalent voltages, V_1 and V_2, which are in turn generated by the motion-induced current. The voltages can be expressed as

$$\frac{V_1}{R_e} + C_{p1}\frac{dV_1}{dt} + \frac{d}{dt}(C_1(x)(V_1 - V_c)) = 0 \quad (2)$$

$$\frac{V_2 - V_{dc}}{R_L} + C_{p1}\frac{dV_2}{dt} + \frac{d}{dt}(C_2(x)(V_2 - V_c)) = 0 \quad (3)$$

The solutions to Eq. (2) and (3) are given by

$$\begin{aligned} V_1(t) = C_1(t)v_c(&\omega_c(\beta_{\omega_c,1}cos(\omega_c t + \phi) - \alpha_{\omega_c,1}sin(\omega_c t + \phi)) \\ &+ \frac{x}{2g}\omega(\alpha_{\omega_+,1}cos(\omega_+ t + \phi) + \beta_{\omega_+,1}sin(\omega_+ t + \phi) \\ &+ \alpha_{\omega_-,1}sin(\omega_- t + \phi) + \beta_{\omega_-,1}cos(\omega_- t + \phi))) \end{aligned}$$

$$\begin{aligned} V_2(t) = C_2(t)v_c(&\omega_c(\beta_{\omega_c,2}cos(\omega_c t + \phi) - \alpha_{\omega_c,2}sin(\omega_c t + \phi)) \\ &- \frac{x}{2g}\omega(\alpha_{\omega_+,2}cos(\omega_+ t + \phi) + \beta_{\omega_+,2}sin(\omega_+ t + \phi) \\ &+ \alpha_{\omega_-,2}sin(\omega_- t + \phi) + \beta_{\omega_-,2}cos(\omega_- t + \phi))) + V_{dc} \end{aligned}$$

with

$$\alpha_{\omega_i,1} = \frac{R_e}{1 + R_e^2 C_{t1}^2 \omega_i^2}, \quad \alpha_{\omega_i,2} = \frac{R_L}{1 + R_L^2 C_{t2}^2 \omega_i^2}$$

$$\beta_{\omega_i,1} = \frac{R_e^2 C_{t1}\omega_i}{1 + R_e^2 C_{t1}^2 \omega_i^2}, \quad \beta_{\omega_i,2} = \frac{R_L^2 C_{t2}\omega_i}{1 + R_L^2 C_{t2}^2 \omega_i^2}$$

where $C_{t1} = C_{p1} + C_1$ and $C_{t2} = C_{p1} + C_2$. The coefficient ω_i in $i = c$, $+$, and $-$ cases denote the frequencies of ω_c, $\omega_c + \omega_d$, and $\omega_c - \omega_d$, respectively. These equivalent voltages lead to forces applied to the mechanical system via the coupling capacitances. The corresponding forces can be expressed as

$$\begin{aligned} F_e(x) &= F_{e1} + F_{e2} \\ &= \frac{C_1(t)}{2g(1 - x_n)^2}(V_c - V_1)^2 - \frac{C_2(t)}{2g(1 + x_n)^2}(V_c - V_2)^2 \end{aligned}$$

Expanding the equation and keeping the terms at ω and 2ω frequencies would yield a set of harmonic force terms that depend on the position and velocity. Then, substituting the corresponding equations for forces in Eq. (1) yields the equation of motion

$$\begin{aligned} m\ddot{x} + (b + b_1)\dot{x} + (k + k_{e0} + k_{e1}sin(\omega t) + k_{e2}sin(2\omega t) + \\ k_{e3}cos(2\omega t))x = F_{th} + F_{e0} \end{aligned} \quad (4)$$

Here, k_{e0}, k_{e1}, k_{e2}, and k_{e3} are the electrostatic spring stiffnesses caused by the harmonics forces. b_1 is the electrical damping, which is given by

$$b_1 = \frac{1}{2}\Lambda_1 v_c(\alpha_{\omega_+,1} + \alpha_{\omega_-,1}) + \frac{1}{2}\Lambda_2 v_c(\alpha_{\omega_+,2} + \alpha_{\omega_-,2}) \quad (5)$$

with

$$\Lambda_1 = \frac{1}{2}\frac{C_{1,x=0}^2}{g^2}v_c, \quad \Lambda_2 = \frac{1}{2}\frac{C_{2,x=0}^2}{g^2}(v_c + V_{dc}) \quad (6)$$

The Q-factor of a resonator is inversely proportional to the energy dissipated per cycle, $E_{Loss} = \int_0^{\frac{2\pi}{\omega}} b\,\dot{x}xdt = \pi b\omega$, due to viscous damping. With the electrical damping and excitation applied in the EAM scheme, the energy per cycle is modified, resulting in an effective Q-factor given by

$$Q_{eff} = Q_0 \frac{\pi\, b\, \omega}{\pi(b + b_1)\omega - \frac{1}{2}\pi(k_{e1} + k_{e2})} \quad (7)$$

B. Comparison of Modeling and Experimental Data

The derived analytical model can be expanded to the dynamically amplified dual-mass gyroscope (DAG), shown in Fig. 1. The DAG is a dual-mass spring structure [8], [9], which comprises an inner drive-mass (m_1) attached to a central anchor and connected to an outer sense-mass (m_2) by concentric ring suspensions (k_1 and k_2). Fig. 3 is the equivalent system of the DAG based on the configuration of the drive, pick-off, and tuning electrodes. V_{t1} and V_{t2} are the DC tuning voltages representing the electrostatic compensation method used in operation of the DAG [13].

The sensor has a resonance frequency of 4.4 kHz. The designed capacitance of each inner and outer electrodes and parasitic capacitance are 1.2, 1.64, and 3.3 pF, respectively. The DAG was vacuum packaged [14] and experimentally measured with the quality factors at 146k and 205k along

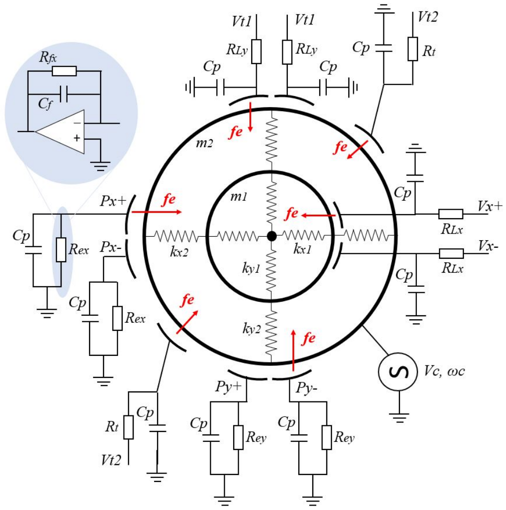

Fig. 3. The electro-mechanical schematics of DAG. An AC carrier signal with V_c in voltage and ω_c in frequency is applied to the gyroscope's proof-mass. Two TIAs with the feedback resistances, R_{fx} and R_{fy}, are used to collect the motional currents from the pick-off electrodes, P_{x+}, P_{x-}, P_{y+}, and P_{y-}. Parameters R_{ex} and R_{ey} denote the effective equivalent loads caused by the feedback resistances and TIAs. R_t, R_{Lx}, and R_{Ly} are the loading resistances on the corresponding tuning and driving electrodes.

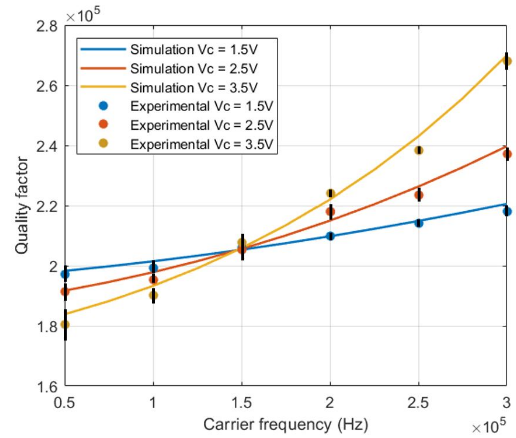

Fig. 4. The simulated Q-factors (in solid lines) of the DAG using the derived analytical model at different carrier voltages from 1.5 to 3.5 V. The dotted lines with black error bars are experimental results at different carrier voltages and show good agreement with the simulated trend in the Q-factor as a function of the carrier frequency.

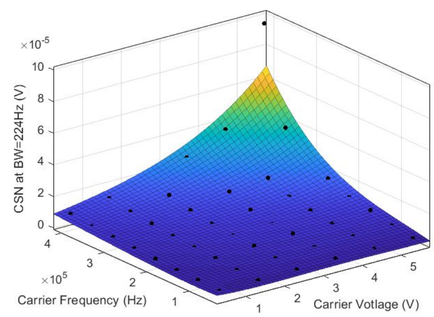

Fig. 5. The operational amplifier noise (OAN) measured with 224 Hz bandwidth under different carrier voltages and carrier frequencies, from 0.5 to 5.5 V and 50 to 400 kHz. The 4×4 polynomial surface fitting was used to simulate the OAN from our experimental setup.

the drive (x) and sense (y) axes. The sensor was assembled on a front-end circuit board placed in a temperature chamber providing a stable temperature during experiments ($<$ 0.5 deg fluctuation). 500 kOhm feedback resistances of the transimpedance amplifier, R_{fx} and R_{fy}, were used at the pick-off channels of the circuit. The gyroscope was operated at the resonance frequency controlled by a Phase-Locked Loop. The drive amplitude was at 1% of the electrode gap.

The effective Q-factors in the experiment were all obtained by using ring-down measurements [15]. The simulation results obtained using the developed electrical dissipation model and the corresponding experimentally measured Q-factors of the DAG along the y-axis are presented in Fig. 4. It shows a clear influence of varying carrier frequencies on the Q-factor, suggesting that the voltage and frequency of the bias signal in EAM play an important role in determining the effective Q-factor and can be potentially used for improvements in gyroscope sensitivity.

III. EAM Noise Analysis

The use of the amplitude and frequency of the AC carrier signal demonstrated in the previous section presented an opportunity to regulate the Q-factor. In addition, these parameters also affect different noise components and signal-to-noise ratio (SNR) in the open-loop rate mode operation of MEMS CVGs.

There are many sources of noise in CVGs with capacitive detection, including electronic-thermal noise (ETN), flicker noise (FN), and operational amplifier noise (OAN). OAN is an output noise from the TIA of the front-end circuit. It is equivalent to adding a noise to the gyroscope pick-off signal. The noise level of the OAN was measured and is illustrated in Fig. 5. In a subsequent experiment, the OAN shows a significant increase in the high frequency and high voltage range.

The gyroscope rate equivalent noise represented by angle random walk (ARW) can therefore be calculated using the gyroscope scale factor, $SF = SF_{ele} \times SF_m$. It is determined by the EAM scheme and by the gyroscope dynamics [2]:

$$SF_m = \frac{2A\alpha\omega_x}{\sqrt{(\omega_y^2 - \omega_x^2)^2 + (2\mu_y\omega_x)^2}} \tag{8}$$

$$SF_{ele} = \frac{1}{2}R\frac{c_s}{g}V_c \times (\omega_c + \omega_x) \tag{9}$$

where SF_{ele} is the pick-off electronics scale factor in V/m, and SF_m is the scale-factor calculated from sensor dynamics in m/(rad/s). A, α, R, c_s, and μ_y are the drive amplitude, angular gain, feedback resistance, nominal capacitance of pick-off electrodes, and damping coefficient, respectively.

The schematic of the MEMS CVGs noise model is illustrated in Fig. 6. The parameters in the model were all obtained experimentally. Estimation of the ARWs of the DAG using the derived noise model was performed as a function of the carrier frequency from 50 to 300 kHz at different carrier voltages from 1.5 to 3.5 V, shown in Fig. 7(a). This reveals a good agreement with the experimental data, validating the developed mathematical model. A full range ARW prediction of the DAG

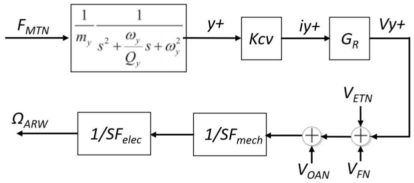

Fig. 6. Schematics of the noise model in MEMS CVGs. G_R was the TIA gain and K_{CV} is the displacement-to-voltage transfer coefficient in EAM.

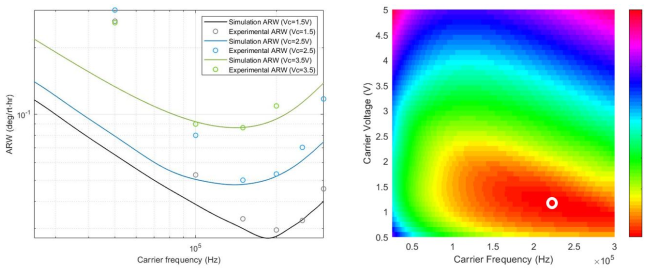

(a) (b)

Fig. 7. (a) The estimated ARWs (in solid lines) of the DAG using the noise analysis model and the experimental results (in circular points). The frequency splits were remained at 1.25 Hz for all the cases. The DAG was actuated at the maximum amplitude without modifying the readout signal due to the 2 Vpp limit of the maximum input voltage of the Zurich HF2LI lock-in amplifier, which was used in our experimental setup. (b) The full range ARW estimation using the noise analysis model. The circular data point is the lowest ARW which occurs around 1.2 V carrier voltage and 225 kHz carrier frequency.

from 0.5 to 7 V carrier voltage and 25 to 300 kHz carrier frequency, shown in Fig. 7(b), suggests the optimized noise performance of the DAG appeared around 1.2 V and 225 kHz carrier voltage and frequency, respectively. The root-PSD of the noise characterization using the suggested parameters is shown in Fig. 8, which experimentally demonstrated an improved performance of the DAG, with 0.08 deg/hr in bias instability and 0.0065 deg/rt-hr in ARW.

IV. Conclusion

The effect of EAM on MEMS CVG performance was theoretically predicted and experimentally demonstrated on the DAG in open-loop rate mode of operation. Analytical equations were derived for simulation of the effect of EAM on the effective quality factor and electrical dissipation. A good agreement between the experimentally measured Q-factors and simulation results were observed for the DAG. We concluded that the AC carrier signal in EAM presented a clear method of tuning the effective Q-factor in MEMS CVGs. We also studied the impact of EAM in gyroscope output noise and demonstrated a 6× improvement of noise performance of the DAG when utilizing the optimized EAM parameters.

Acknowledgment

This material is based on work supported by the Defense Advanced Research Projects Agency and U.S. Navy under contract No. N66001-16-1-4021. Devices were designed and characterized at UCI Microsystems Laboratory and fabricated at UCI INRF cleanroom facility. The authors would like to acknowledge Austin Roger Parrish and Yi Zhuang from MicroSystems lab for valuable contribution during the study.

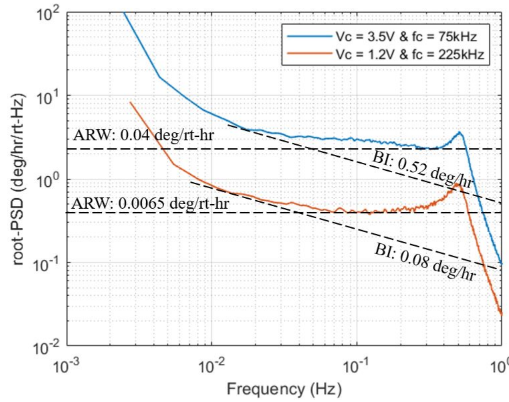

Fig. 8. Shown is the root-PSD plot of the DAG zero rate output operated in open-loop rate mode with an electrostatically tuned frequency spilt at 0.5 Hz.

References

[1] C. C. Nguyen, "Micromechanical signal processors." Ph.D. dissertation, University of California, Berkeley, 1994.

[2] A. A. Trusov and A. M. Shkel, "A novel capacitive detection scheme with inherent self-calibration," *IEEE Journal of Microelectromechanical Systems*, vol. 16, no. 6, pp. 1324–1333, 2007.

[3] J. Cao and C. T.-C. Nguyen, "Drive amplitude dependence of micromechanical resonator series motional resistance," in *Digest of Technical Papers, 10-th International Conference on Solid-State Sensors and Actuators, Sendai, Japan, June 7*, vol. 10. Citeseer, 1999.

[4] H. Cao, H. Li, J. Liu, Y. Shi, J. Tang, and C. Shen, "An improved interface and noise analysis of a turning fork microgyroscope structure," *Mechanical Systems and Signal Processing*, vol. 70, pp. 1209–1220, 2016.

[5] J. Xie, Y. Hao, and W. Yuan, "Energy loss in a mems disk resonator gyroscope," *Micromachines*, vol. 10, no. 8, p. 493, 2019.

[6] N. E. Bousse, J. M. Miller, H.-K. Kwon, G. D. Vukasin, and T. W. Kenny, "Quality factor tuning of micromechanical resonators via electrical dissipation," *Applied Physics Letters*, vol. 116, no. 2, p. 023506, 2020.

[7] C. C. Painter and A. M. Shkel, "Dynamically amplified rate integrating gyroscope," Aug. 16 2005, US Patent 6,928,874.

[8] D. Wang, M. H. Asadian, A. Efimovskaya, and A. M. Shkel, "A comparative study of conventional single-mass and amplitude amplified dual-mass MEMS Vibratory Gyroscopes," in *IEEE International Symposium on Inertial Sensors and Systems (INERTIAL)*, Kauai. HI, USA, March 27-30 2017.

[9] D. Wang, A. Efimovskaya, and A. M. Shkel, "Amplitude Amplified Dual-Mass Gyroscope: Design Architecture and Noise Mitigation Strategies," in *IEEE International Symposium on Inertial Sensors and Systems (INERTIAL)*, Naples. FL, USA, April 1-5 2019.

[10] G. Jourdan, G. Torricelli, J. Chevrier, and F. Comin, "Tuning the effective coupling of an afm lever to a thermal bath," *Nanotechnology*, vol. 18, no. 47, p. 475502, 2007.

[11] A. Cleland and M. Roukes, "External control of dissipation in a nanometer-scale radiofrequency mechanical resonator," *Sensors and Actuators A: Physical*, vol. 72, no. 3, pp. 256–261, 1999.

[12] R. Gando, S. Maeda, K. Masunishi, Y. Tomizawa, E. Ogawa, Y. Hatakeyama, T. Itakura, and T. Ikehashi, "A mems rate integrating gyroscope based on catch-and-release mechanism for low-noise continuous angle measurement," in *2018 IEEE Micro Electro Mechanical Systems (MEMS)*, Belfast, Ireland, Jan. 21-25 2018.

[13] A. Efimovskaya, D. Wang, Y.-W. Lin, and A. M. Shkel, "Electrostatic compensation of structural imperfections in dynamically amplified dual-mass gyroscope," *Sensors and Actuators A: Physical*, vol. 275, pp. 99–108, 2018.

[14] M. H. Asadian, S. Askari, and A. M. Shkel, "An ultrahigh vacuum packaging process demonstrating over 2 million q-factor in mems vibratory gyroscopes," *IEEE sensors letters*, vol. 1, no. 6, pp. 1–4, 2017.

[15] J. M. L. Miller, A. Ansari, D. B. Heinz, Y. Chen, I. B. Flader, D. D. Shin, L. G. Villanueva, and T. W. Kenny, "Effective quality factor tuning mechanisms in micromechanical resonators," *Applied Physics Reviews*, vol. 5, no. 4, p. 041307, 2018.